

Investigation of High Power Impulse Magnetron Sputtering deposited nanoscale CrN/NbN multilayer coating for tribocorrosion resistance

PURANDARE, Yashodhan <<http://orcid.org/0000-0002-7544-9027>>, ROBINSON, G.L., EHIASARIAN, A.P. and HOVSEPIAN, P. Eh

Available from Sheffield Hallam University Research Archive (SHURA) at:

<https://shura.shu.ac.uk/26187/>

This document is the Accepted Version [AM]

Citation:

PURANDARE, Yashodhan, ROBINSON, G.L., EHIASARIAN, A.P. and HOVSEPIAN, P. Eh (2020). Investigation of High Power Impulse Magnetron Sputtering deposited nanoscale CrN/NbN multilayer coating for tribocorrosion resistance. *Wear*, p. 203312. [Article]

Copyright and re-use policy

See <http://shura.shu.ac.uk/information.html>

Investigation of High Power Impulse Magnetron Sputtering deposited nanoscale CrN/NbN multilayer coating for tribocorrosion resistance

Y.P. Purandare, G.L. Robinson, A.P. Ehiasarian and P. Eh. Hovsepian
National HIPIMS Technology Centre, MERI, Sheffield Hallam University, UK

Abstract

Recycling equipment (waste/ sea water/chemicals) need high tribocorrosion resistance. In this work High Power Impulse Magnetron Sputtering technique deposited nanoscale CrN/NbN multilayer coating for tribocorrosion resistance is explored. Sliding-wear experiments were conducted on CrN/NbN coated High Speed Steel (HSS) test coupons with an alumina (Al_2O_3) ball as a counterpart in a corrosive environment (3.5% NaCl solution) under potentiodynamic and potentiostatic conditions. Results reveal that coated substrates exhibited (by a factor of 3) lower corrosion currents and high tribo-corrosion resistance ($K_c = 2 \times 10^{-15} \text{ m}^3\text{N}^{-1}\text{m}^{-1}$) as compared to uncoated HSS specimens. The alumina counterpart exhibited negligible wear in all the tests. Superior adhesion and dense microstructure consisting of flat and well-defined hard nitride nanolayers leads to stable friction coefficients and retain the unique nanoscale layer-by-layer wear mechanism without delamination. Effect of corrosion on friction coefficients, wear mechanisms and vice versa has been presented.

Key words: HIPIMS; tribocorrosion resistance; nanoscale multilayers; CrN/NbN.

1.0 Introduction:

Losses from wear and corrosion of components are a major cause of concern for industries. Wear and corrosion, when acting separately are in themselves destructive in nature. It is also now widely established that when these phenomenon combine (described as tribocorrosion), due to the synergy between them, more severe wear mechanisms dictate and in most cases intensify the damage [1-6]. In real world environments, tribo-corrosive conditions are omnipresent. Increasing awareness towards greener technologies and environmental protection has led to an increase in the efforts to recycle water and waste. In such scenarios, industries will have to deal with working conditions where tribo-corrosive mechanisms reign. The surfaces in service should possess high wear as well as high corrosion resistance however should also retain these properties in tribocorrosive conditions. A suitable way to address this problem is to employ a surface coating with the requisite attributes.

For most metals and alloys, total wear due to tribocorrosion can be expressed as:

$$V_T = V_M + V_C + \Delta V_S \quad (1)$$

where, V_T = total wear in tribocorrosive conditions, V_M = wear due to mechanical action, V_C = wear due to corrosion and ΔV_S = the interaction between wear and corrosion [7, 8]. In most cases ΔV_S is synergistic i.e. it has a positive effect leading to enhanced wear and can be resolved further as [7]:

$$\Delta V_S = \Delta V_W + \Delta V_C \quad (2)$$

where ΔV_W = corrosion induced wear and ΔV_C = wear induced corrosion.

In the case of a coating, the term ΔS can become more complex. Various factors such as substrate adhesion, microstructural density and defects, its inherent hardness, toughness and

corrosion resistance will play a significant role in determining the synergy. For example, a structure not fully dense or a defect will cause corrosion of the substrate, which in-turn will lead to delamination of the coating. The delaminated coating will act as wear debris, increasing friction and wear due to 3 body abrasion mechanisms.

Physical Vapour Deposition (PVD) technique deposited CrN/NbN nanoscale multilayer coatings offer a suitable choice for such complicated applications [9]. The modulation of nanoscale chromium nitride (CrN) and niobium nitride (NbN) layers impart high hardness and toughness which lead to greatly enhanced dry sliding wear resistance as well as corrosion resistance (wet and high temperature oxidation) [9-11]. Recently established High Power Impulse Magnetron Sputtering (HIPIMS) technology is a highly ionised deposition process [12, 13] which can deposit coatings that are droplet-defect free [14], structurally dense, architecturally superior (compositionally defined and flat interfaces between nanolayers) and with high adhesion [15]. The resultant superior microstructure enhances the barrier properties of the coating to a great extent [16, 17]. The introduction of the HIPIMS technique to deposit CrN/NbN coatings led to a big improvement in its dry sliding wear resistance and aqueous corrosion resistance [16], abrasive particle impact erosion-corrosion resistance [18] as well as steam oxidation resistance [19, 20].

This study investigates the suitability of a HIPIMS deposited nanoscale CrN/NbN coating for tribo-corrosive applications. The performance of this coating in an atmosphere comprised of combined sliding wear and aqueous corrosion has been thoroughly investigated for the first time. Emphasis has been placed on studying the effect of corrosion on the gradual layer by layer removal mechanism of these coatings or vice-versa by analysing its effect on friction coefficients, wear coefficients and wear mechanisms at a wider range of corrosion conditions. Raman spectroscopy has been used to analyse the corrosion products that may form during the

sliding process. The benefits of the CrN/NbN coating have been further investigated by comparing its performance against uncoated High Speed Steel (HSS) substrates.

2.0 Experimental:

2.1 Coating deposition:

The CrN/NbN coatings were deposited in the Nanotechnology Centre for PVD Research based at Sheffield Hallam University, Sheffield UK. The coatings have been deposited on polished (1 micron finish) M2 High Speed Steel (HSS) coupons (elements by weight percent (wt. %) - C: 0.85, Mn: 0.28, Si: 0.30, Cr: 4.15, W: 6.15, Mo: 5, V: 1.85, Rest Fe) with the help of HIPIMS technology. It consists of a base layer of CrN (around 0.25 μ m) followed by an uninterrupted growth of alternating nano layers of CrN and NbN at a bias voltage of -65 V in 2 fold rotation to yield a multilayer coating. The synthesis was carried out with the help of two targets (Cr and Nb with a purity of 99.9%) operating in HIPIMS mode along with other two (Cr and Nb) in UBM-DC mode. The sputtering targets were operated at a constant power mode with an average power on the individual cathode at 8 kW irrespective of the technology (UBM or HIPIMS). The HIPIMS power supply parameters yielded rectangular pulses of 200 μ s at a frequency of 100 Hz, with a duty cycle of 1 %. During deposition Ar and N₂ (1:1) were used as process gasses (chamber pressure in the range of 3 x 10⁻³ mbar) whereas a constant temperature of 400 °C was maintained throughout the deposition. Further details of the deposition chamber, substrate table and the process parameters can be found in the literature [16]. In order to compare the performance, experiments were also conducted on uncoated polished (1-micron finish) M2 HSS coupons.

2.2 Coating characterisation:

The coatings were thoroughly characterised to measure their mechanical properties such as nano-hardness, adhesion (L_{C2}) and sliding wear coefficients (K_c). The nanoscale multilayer structure was characterised by X-ray diffraction techniques (Empyrean diffractometer, PANalytical, The Netherlands). Low angle ($2\theta^\circ$, 1° - 10°) Bragg-Brentano geometry was used for bi-layer period measurement whereas a glancing angle technique was used to study stress and preferred orientation of the texture of the coatings. A Scanning Electron Microscope (NOVA-NANOSEM 200, FEI, The Netherlands) was used in the secondary electron imaging mode to capture images of the coating microstructure as well as to image test generated wear tracks. A Transmission Electron Microscope (TEM) (EM420, Phillips, The Netherlands) was operated in a bright field imaging mode to capture the cross-sectional view of the multilayer structure. Coating adhesion (critical load (L_{C2}) of coating failure) was measured with a scratch tester (REVETEST, Anton Paar-CSM instruments, Switzerland) under progressive loading conditions whereas a nanoindenter with a Berkovich tip (NHT, Anton Paar-CSM instruments, Switzerland) was used to measure hardness and Young's modulus of the nanolayers [21]. A stylus profilometer (Dektak-150, Veeco Instruments, USA) was used to profile wear tracks generated.

The corrosion products on the wear tracks were analysed with the help of a Raman spectrometer (LabRam HR800, Horiba-Jobin-Yvon, France) fitted with a green laser ($\lambda = 532$ nm, 5 mW output power). The samples were rinsed with de-ionised water followed by hot air drying before conducting Raman spectroscopy. The spectra were collected with a Lab-Spec software (version V5 embedded into the spectrometer system) which was also used to correct for the background noise, de-spike and smooth the data whereas a multi-peak Gaussian-fitting function was used to de-convolute the spectra and identify the Raman peaks. The spectra were averaged over 3 acquisitions in the wavelength range of $100 - 1600$ cm^{-1} .

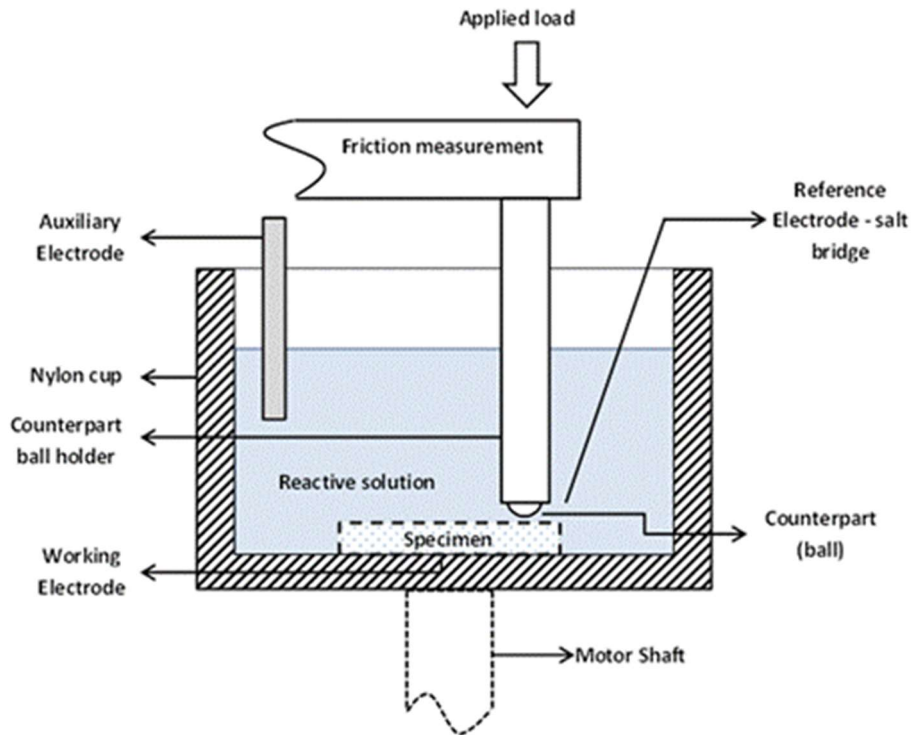


Figure1: Schematic representation of the Sliding wear-corrosion set up.

2.3 Sliding wear – corrosion (SWC) experiments:

Sliding wear-corrosion experiments were conducted on a pin on disk tribometer (Room temperature tribometer, Anton Paar- CSEM Instruments, Switzerland) which was modified to incorporate in-situ corrosion analysis. The apparatus consists of a chemically inert static pin (6 mm Al_2O_3 ball-hardness 1800 HV) in contact with a rotating specimen held submerged in the corrosive liquid. Figure 1 shows the schematic of the apparatus which forms a 3 electrode corrosion cell consisting of an exposed area of the specimen as a working electrode and a carbon rod as auxiliary electrode. A saturated silver/silver chloride (Ag/AgCl) electrode was used as a reference electrode. All the electrochemical potentials mentioned are with respect to the Ag/AgCl reference electrode. Corrosion conditions were held and monitored with the help of a potentiostat (Gill AC, ACM instruments, UK).

In this study a 3.5% sodium chloride (NaCl) aqueous solution ($\text{pH} = 7$) was used as the corrosive medium. A vast research data on dry sliding wear rate and wear mechanisms of nanoscale multilayer coatings deposited by HIPIMS, d.c magnetron sputtering and cathodic arc techniques at Sheffield Hallam University, and particularly on CrN/NbN multilayer coatings has been published before. Hence, being consistent with previous research articles, test parameters comprising of 5N static normal load, alumina counterpart (Hertzian contact pressure in the range of 1.5 GPa in static mode) and a linear sliding velocity of 0.1ms^{-1} were employed in this study. These test parameters will facilitate a direct comparison of the coating performances (in dry and tribo-corrosive atmospheres) and gauge the benefits of employing HIPIMS for deposition.

In order to examine tribo-corrosive response of the specimens thoroughly, these experiments were conducted in potentiodynamic and potentiostatic conditions. The samples were masked with a non-conductive lacquer to expose a limited area to the corrosive solution and the rubbing action of the ball. Depending on the experimental setup, the exposed area was in the range of 0.8 to 1.6 cm^2 . To investigate the effect of wear on phenomenon such as E_{CORR} values, anodic and passivation corrosion kinetics, potentiodynamic conditions were coupled with sliding wear. During these experiments, the electrochemical potential was varied from -1000 mV to +1000 mV (with respect to Ag/AgCl reference electrode) at a sweep rate of 1mVs^{-1} resulting in a total distance of approximately 178 m. Pilot studies on HSS specimens exhibited a strong tendency of the alloy to form corrosion products in the stipulated test period. Hence, for potentiostatic experiments, a sliding distance of 150 m was chosen to avoid saturation of the test solution with corrosion products and thereby influence test results. Three potentiostatic potentials were chosen; one for a condition representing dominating wear conditions (cathodic potential/ immunity to corrosion of -1200 mV) and two in the anodic potentials (+100 mV and +600 mV). Following the tests, samples were rinsed with de-ionised water and dried with a hot

air blower. The cross-sectional area of the wear tracks was measured using the stylus laser profilometer. At least four measurements were taken on each wear track at 90° apart. Wear coefficients, K_c (total wear due to combined sliding action and corrosion, $\text{m}^3\text{N}^{-1}\text{m}^{-1}$), were calculated using the following formula:

$$K_c = \frac{A_t \cdot v}{F_N \cdot L} \quad (3)$$

where, A_t is the cross-sectional area of the wear track, v is the linear velocity, F_N is the normal load in Newton and L is the number of laps. Each test was repeated three times to find its repeatability.

3.0 Results and Discussion:

3.1 Characterisation results:

Figure 2a shows the as-deposited surface of the coating whereas figure 2b shows the cross-section of the coating deposited on Si substrates. As evident from the SEM image (figure 2b), the HIPIMS deposited coating consisted of very dense columnar grains (around 100-250 nm wide) which are formed by the alternate stacking of nanoscale CrN and NbN layers (figure 2c). These columnar grains terminated into dome-shaped tops (figure 2a) which are typical of magnetron sputtered coatings, albeit very densely packed. The microstructure is free of any droplet defects often seen in popular cathodic arc deposition technique for PVD coatings [14]. The CrN/NbN coatings used in this study had an f.c.c (Fm3m) NaCl crystal structure, thickness in the range of $7 \pm 0.3 \mu\text{m}$ with a bi-layer period (λ) of 4.6 nm and a roughness value (Ra) of 0.16 μm . The coatings were found to be stoichiometric ($\text{Me}/\text{N} = 1$). The coatings had a high scratch adhesion (L_{C2}) in excess of 80 N, high hardness of $32 \pm 1.3 \text{ GPa}$, Young's Modulus of

406 ± 11 GPa and a compressive stress of 4 ± 0.2 GPa. M2 HSS specimens had a hardness of 14 ± 0.4 GPa (Rockwell hardness of RC 56), Young's modulus of 270 ± 5 GPa whereas the surface roughness (Ra) was in the range of $0.013 \mu\text{m}$.

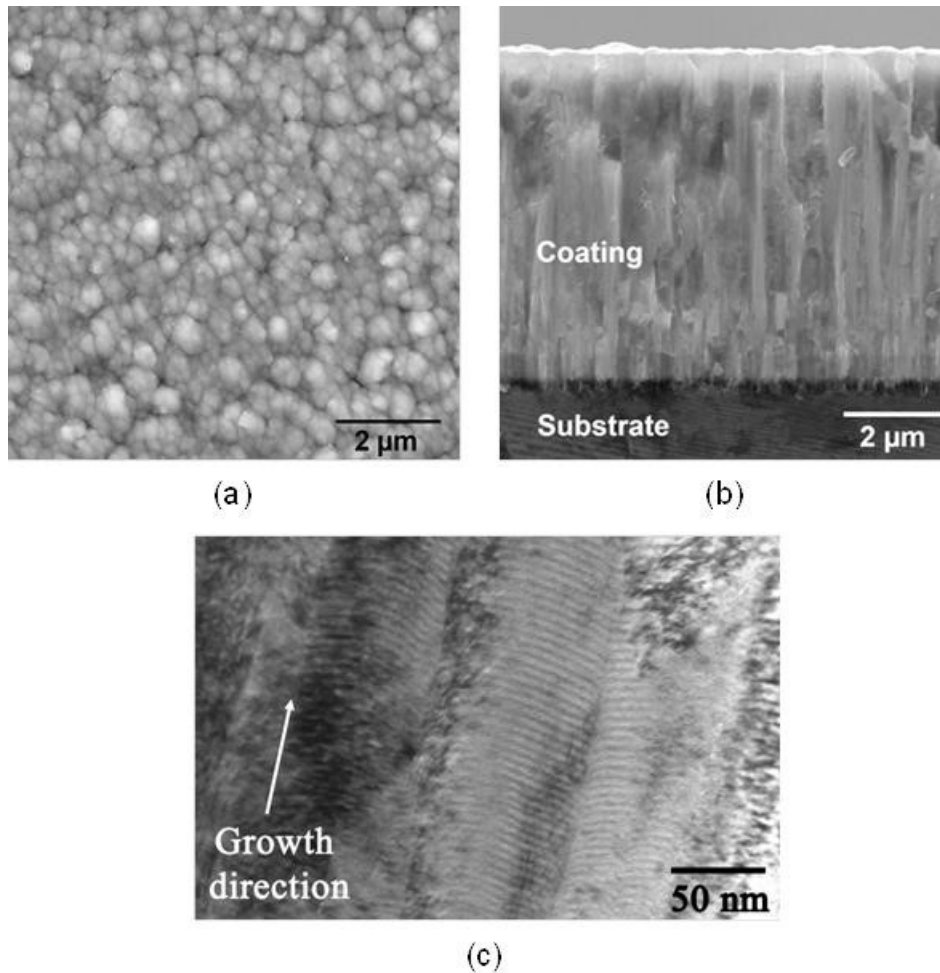


Figure 2: CrN/NbN coating structure: (a) plan view SEM image of the as deposited surface (b) SEM image of the cross-sectional view (c) bright field TEM image exhibiting alternating nanoscale CrN (light contrast area) and NbN (dark contrast) layers.

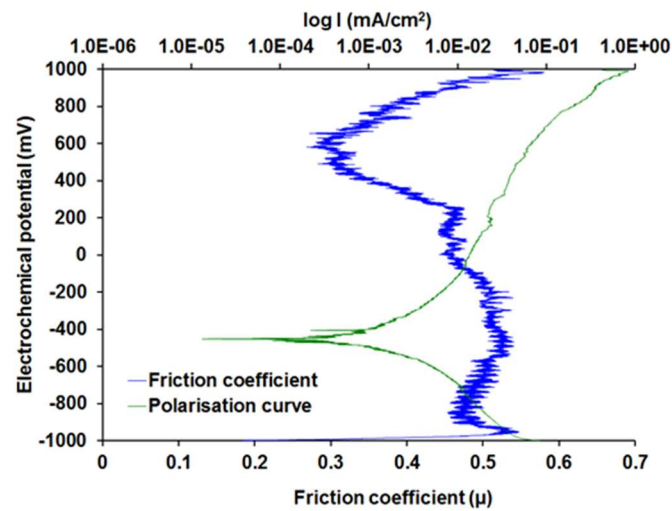
3.2 Sliding wear-corrosion results:

Previous work on dry sliding wear of HIPIMS deposited CrN/NbN coating showed that the nanoscale multilayer coating had a superior layer by layer removal mechanism [16, 22] which

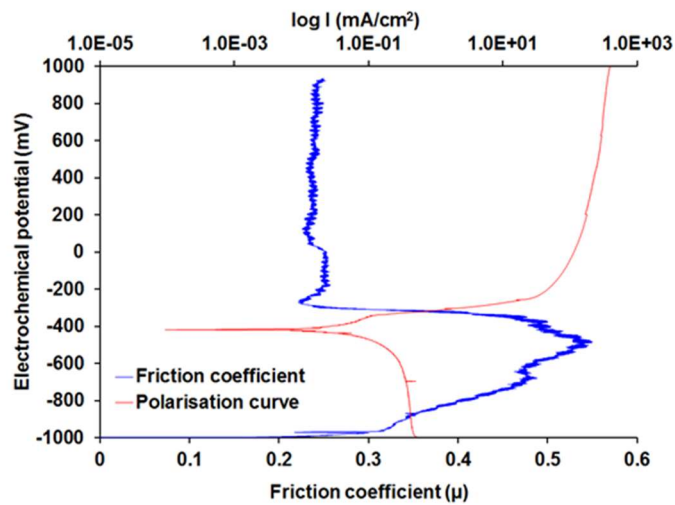
led to a friction coefficient value in the range of $\mu = 0.3 - 0.5$ [16, 18]. To understand the effect of aqueous corrosion on the wear resistance and vice-versa, sliding wear-corrosion experiments were conducted in potentiodynamic as well as potentiostatic conditions.

3.2.1 Potentiodynamic conditions:

Figure 3(a-b) shows the polarisation curves along with the friction coefficient of the coating and the HSS specimen recorded as a function of sliding distance (total 178 m) and changing electrochemical potentials when tested in 3.5% NaCl solution.



(a)



(b)

Figure 3: Polarisation curves, friction coefficient measurement as a function of sliding distance under a normal load of 5N (a) CrN/NbN coating (b) M2 HSS specimen.

Under the SWC conditions, CrN/NbN coating and the HSS specimens exhibit an E_{Corr} value of -455 mV and -418 mV respectively. As anticipated, due to the difference in their corrosion resistance, the results indicate a significant difference between the behaviour of the two samples.

The CrN/NbN coated substrate showed a near similar value of friction coefficient (around $\mu = 0.48$) in the cathodic potential range (figure 3a). In the anodic potential range of -455 mV and +250 mV, the friction coefficient decreased gradually from $\mu = 0.51$ to around $\mu = 0.46$. The outermost layer of the coating (surface) will either comprise of CrN or NbN depending on the extent of wear caused by the mechanical effect (sliding wear). In this corrosive environment (3.5% NaCl solution) and anodic potentials, chromium was liable to corrode and form different types of oxides depending on the electrochemical potential, whereas niobium oxide (Nb_2O_5) was expected to be electrochemically stable for the whole range studied in this work [23]. Thus, formation of oxides and their removal/dissolution during the sliding process appeared to have an effect [24, 25], albeit small, resulting in lowering the friction coefficient in this potential range.

In the electrochemical potential range of +260 mV to +650 mV, the friction coefficient value dropped steadily to a value around $\mu = 0.27$. In this potential range, chromium shows a tendency to undergo rapid dissolution to form different type of oxides (at relevant potentials) whereas niobium was expected to passivate, comprising of Nb_2O_5 [23]. Thus, the type of corrosion product (chromium oxide: its oxidation state, reactive nature and water solubility) and its dissolution/easy removal (evident from the polarisation curve in figure 3a) during the sliding wear process affects the friction behaviour. Results suggest that these oxides may have been

loosely adhered (see figure 6 and description in section 3.2.2) to the abrading surface and is displaced easily due to the flowing solution providing a lubricating effect.

In the range of +650 mV to +1000 mV potentials, the friction coefficient started to rise and reached values similar to those observed for non-corrosive cathodic conditions. Since passivation of niobium was expected to be continuous and stable in this potential range also, the results suggest that the friction coefficient is again influenced by the change in the nature and composition of chromium oxides in this potential range [23]. Rising friction coefficient value also suggests that these oxides (corrosion products) may have been better adhered to the wear track surface.

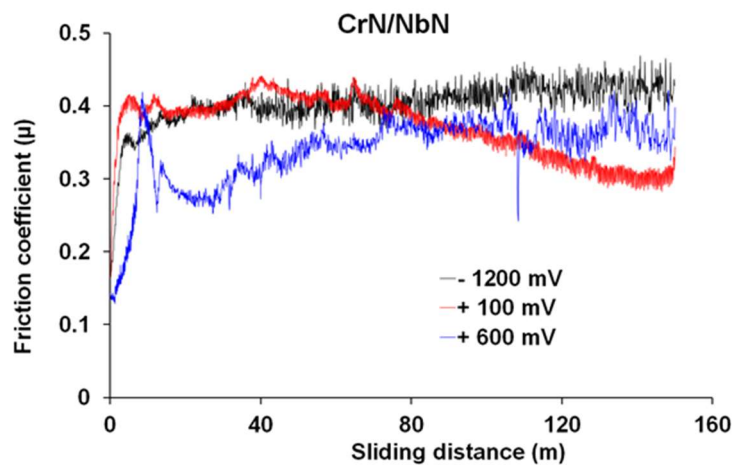
As opposed to the behaviour of coated specimens, the friction coefficient of the HSS specimen showed a continuous change in value with applied electrochemical potentials (figure 3b). Results showed that it increased continuously in the cathodic potential ranges to peak at $\mu = 0.54$ around -470 mV and that the aqueous medium had limited lubrication effect (as compared to dry conditions; see table 1). However, in the anodic potential range of -470 mV to -275 mV it fell sharply to reach a value around $\mu = 0.22$. During this test conditions, the specimen underwent rapid corrosion (evident from the polarisation curve in figure 3(b) and discolouration of the solution). The results suggest that the corrosion products formed on the surface were removed by the sliding action of the ball and displaced from the wear track easily by the flowing solution thus providing a lubricating effect; albeit resulting in heavy wear rate. After an initial increase to $\mu = 0.24$ in the anodic potentials range of -217 mV to -10 mV it stabilised around $\mu = 0.23$ until the end of the experiment. Results suggest that any corrosion products formed on the surface had negligent mechanical integrity and no protective effect against sliding wear and that the mechanism is dominated by rapid formation and removal of the corrosion products/passive layers.

Wear scar profiling showed that, in these tribo-corrosive conditions, the HSS specimen corroded heavily and showed heavy material loss (maximum wear track depth in the range of 20 μm). In comparison, the CrN/NbN coated substrates showed four orders of magnitude lower anodic corrosion currents and very low wear loss and the coating to be intact (maximum wear track depth of 0.53 μm). In all the experiments conducted, the wear on the counterpart (alumina ball) was very minuscule and was difficult to quantify.

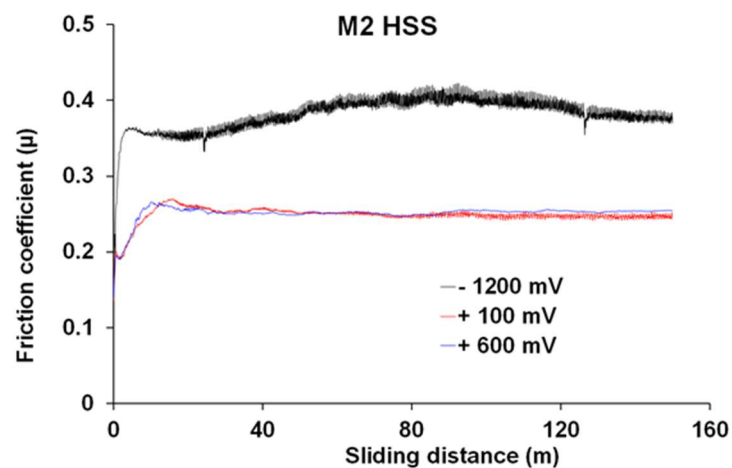
3.2.2 Potentiostatic conditions:

Figure 4a shows the friction coefficients recorded at different corrosion conditions for the coating. In the cathodic conditions of -1200 mV (figure 4a), after the initial run in period, the friction coefficient of the coating stabilised around $\mu = 0.4$ until the end of the experiment. In this condition, no corrosion of the specimen was expected and that the wear mechanism consisted solely of coating removal under aqueous lubrication conditions. During experimentation, continuous circulatory motion of the fluid facilitated easy removal of the wear debris from the wear track. Figure 5a shows the SEM images of this wear track and surrounding as-deposited surface of the coating. In general, the wear track appeared smooth with no abrupt coating delamination (loss of adhesion from the substrate or even due cohesive delamination between individual layers of CrN and NbN). The surfaces of the coatings also have some defects formed due to contamination from the deposition chamber (visible on virgin surfaces of the coating in figure 5a, 5c and 5e) [26]. Evidence of removal of these defects from the wear track (circular areas with dark contrast) along with micro-grooving was observed at higher magnification in figure 5b. These wear track features are typical of the nanoscale CrN/NbN coating's layer by layer removal mechanism encountered and evidenced in dry lubricated conditions [9, 16]. This unique wear mechanism which can be attributed to the superior adhesion of the dense columnar structure, flat nanoscale multilayers with sharp interfaces, its inherent high hardness and engineered toughness which imparts the CrN/NbN coating with a

high wear resistance (K_c around $2 \times 10^{-15} \text{ m}^3\text{N}^{-1}\text{m}^{-1}$). Table 1 gives the values of mean friction coefficients, mean corrosion currents and calculated sliding wear coefficients of the coating and HSS specimens at different electrochemical potentials in detail. The slight increase in wear coefficient as compared to dry sliding conditions ($K_c = 1.3 \times 10^{-15} \text{ m}^3\text{N}^{-1}\text{m}^{-1}$) could be attributed to the easy removal of the wear debris by the flowing liquid, in effect hindering any beneficial effect the tribo films can have in reducing friction and wear.



(a)



(b)

Figure 4: Friction coefficient as a function of electrochemical potentials under sliding wear conditions under a normal load of 5N (a) CrN/NbN coating (b) M2 HSS specimen.

Specimen	Test Condition	Environment	Mean friction coefficient (μ)	Mean corrosion current density (mA/cm^2)	Wear coefficient (K_c) $\text{m}^3\text{N}^{-1}\text{m}^{-1}$
CrN/NbN	Dry	Air (25°C)	0.59 ± 0.14	-	$1.39 \pm 0.17 (x 10^{-15})$
	-1200	3.5% NaCl solution (25°C)	0.42 ± 0.03	-	$2.02 \pm 0.48 (x 10^{-15})$
	+100		0.36 ± 0.02	$1.66 \pm 0.4 (x 10^{-2})$	$2.72 \pm 0.78 (x 10^{-15})$
	+600		0.33 ± 0.005	$1.02 \pm 0.3 (x 10^{-1})$	$9.37 \pm 0.16 (x 10^{-15})$
HSS	Dry	Air (25°C)	0.78 ± 0.01	-	$5.29 \pm 1.4 (x 10^{-15})$
	-1200	3.5% NaCl solution (25°C)	0.37 ± 0.02	-	Not measurable
	+100		0.23 ± 0.005	$5.92 \pm 1.3 (x 10^1)$	$1.06 \pm 0.16 (x 10^{-12})$
	+600		0.23 ± 0.01	$1.11 \pm 0.49 (x 10^2)$	$1.33 \pm 0.12 (x 10^{-12})$

Table 1: Mean friction coefficient, corrosion currents and wear coefficients measured as a function of electrochemical potentials and sliding distance under a normal load of 5N.

In the anodic conditions of +100 mV (active dissolution of Cr), figure 4a, after the initial run-in period, the friction coefficient achieved a steady value of around 0.4 as the sliding distance approached 80 m followed by a steady decrease to around $\mu = 0.3$. Similarly at +600 mV conditions, the friction coefficient showed a steady increase with sliding distance and increasing passive layer thickness to yield a mean value of $\mu = 0.33$. Simultaneously recorded corrosion currents during these experiments also reached steady values as the friction curves stabilised (table 1). Even though the current values show an order of magnitude increase in value (1.66×10^{-2} at +100 mV to $1.02 \times 10^{-1} \text{ mA.cm}^{-2}$ at +600 mV), in general they were very low even though they were subjected to the harsh tribocorrosion environment. In general, the friction coefficient values recorded in potentiostatic conditions were comparable to those recorded in potentiodynamic conditions at the relevant electrochemical potential. The friction coefficients for all the test conditions for coatings appeared noisier and tended to oscillate (small and sharp rise and fall in the value) with sliding distance. These oscillations appeared more pronounced for the +600 mV as compared to the +100 mV test condition. In the absence

of any debris in the wear track, the friction coefficients will be largely influenced by the structural integrity of the nanoscale nitride layers, the interfaces between these layers and any passive layers/ corrosion products it forms. The appearance of the smooth wear scars in the SEM images suggested that similar to dry sliding wear conditions, harsh tribo-corrosive (tribological and extreme corrosion) environment had little effect on the integrity of the CrN/NbN coating microstructure.

Figure 5 (c-d) shows the SEM images of the wear track when analysed at +100 mV. The wear track appeared smoother than at cathodic potentials (faint grooving marks) with no evidence of coating delamination or decomposition of the coating. Some evidence of removal of coating chamber related defects due to the sliding action was visible (area marked as C1). Even though in anodic potentials, the coating shows a high wear resistance ($K_c = 2.7 \times 10^{-15} \text{ m}^3\text{N}^{-1}\text{m}^{-1}$). Figure 5(e-f) shows the wear track at +600 mV. This wear track appeared the smoothest of all three conditions and showed removal of the chamber related defects (marked as C3 and C4). However, no coating delamination due to the substrate corrosion around these areas was visible. Results indicate that these chambers related defects (mainly incorporation of dust from the chamber walls during deposition) had no significant effect on the tribo-corrosion resistance of the coating. As evident from the polarisation curve in figure 3a, at +600 mV the coating underwent cycles of corrosion, passivation (oxides of Cr and Nb) and subsequent removal of the oxides/ corrosion products. This material removal mechanism and the anticipated higher corrosion contribution and higher oxide rebuilding rates at higher anodic potential [27] led to the slight lowering of the wear resistance ($K_c = 9.3 \times 10^{-15} \text{ m}^3\text{N}^{-1}\text{m}^{-1}$) as compared to +100 mV conditions. In both anodic test conditions, the surface of the wear track was smooth indicating that the wear debris was small in size (possibly nanometer size particles) and that the wear progresses gradually by removal of nanoscale layer(s) at a time. This is a significant result, since corrosion can promote the generation of micro-cracks and thus large size wear debris

leading to higher deterioration rates [7] especially around the areas where coating growth is interrupted to form weak areas (i.e. areas around defects, or less dense structures) [18]. The results suggested that the CrN/NbN coating possesses a high tribocorrosion resistance and can be attributed to the hard, corrosion resistant macro-droplet free, dense columnar structure which has a superior adhesive and cohesive strength and that it performs exceptionally well even at extreme anodic potentials. It is significant to mention that all wear craters (irrespective of electrochemical potentials and repetitions) were contained in the coating and did not reach the substrate. Hence the corrosion contributions (barring any contributions from the substrate due to the removal of thorough thickness chamber related defects, if any, in the selectively exposed area) and mechanical wear contributions are dominated by the coating.

In comparison, the HSS specimens exhibited a significant influence of corrosion on the wear resistance. Figure 4b shows the friction coefficients of the HSS specimen recorded as a function of electrochemical potential and sliding distance. At all potentials, after a brief run-in period, the friction coefficients quickly attained a steady value. The friction curve at cathodic conditions of -1200 mV (mean value of $\mu = 0.38$) was noisier as compared to the anodic conditions. Figure 6a shows the wear track generated at -1200 mV at lower magnification whereas figure 6b shows it at higher magnification. The track appeared rough and had deep groove marks created by the ploughing action (2 body abrasion) of the counterpart and the wear debris. Even though evident, the rough and irregular surface around the grooves and the build-up of material around them due to plastic deformation made wear track profiling and calculation of the wear coefficient difficult.

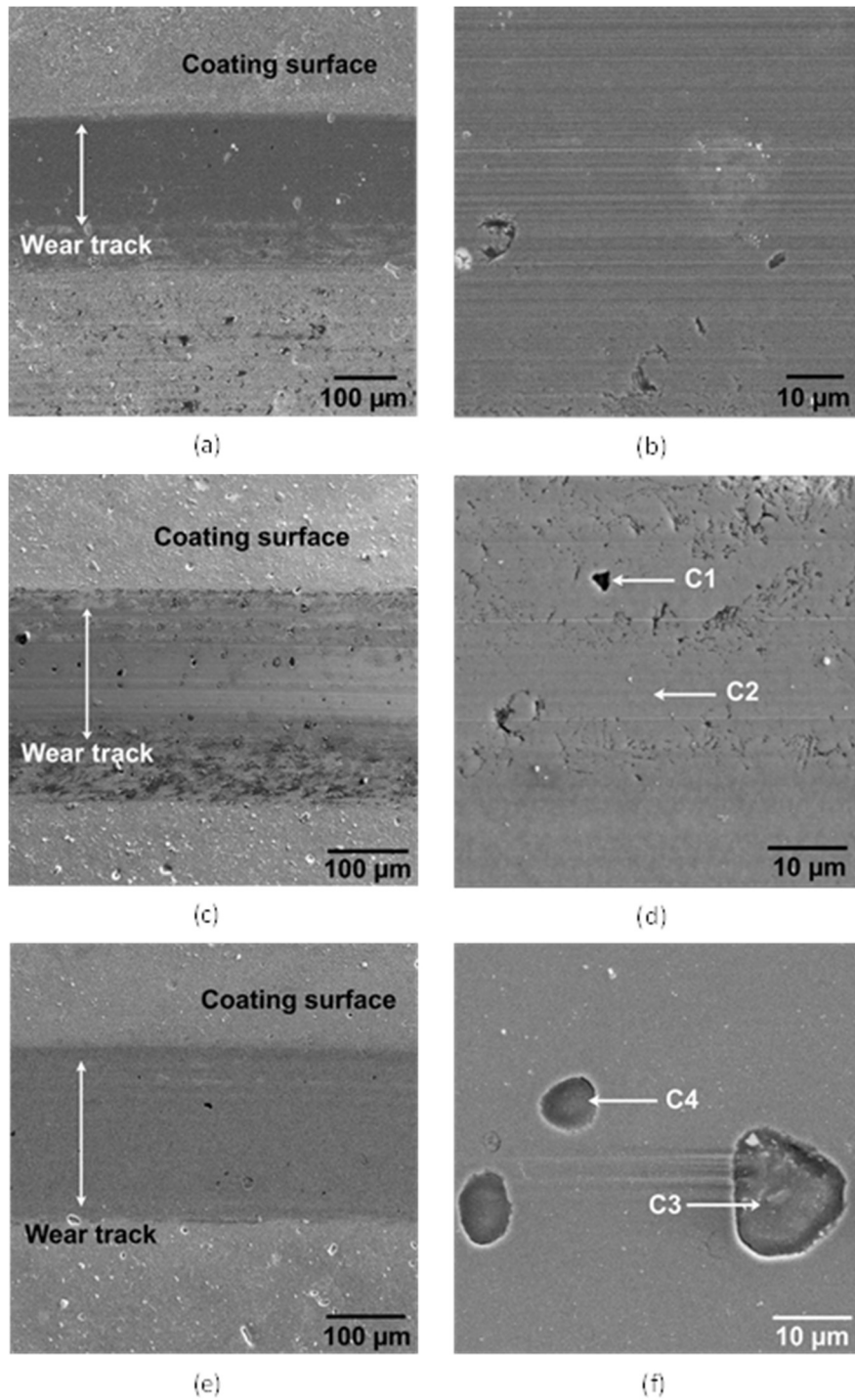


Figure 5: SEM images of the wear tracks on the CrN/NbN coating: (a) -1200 mV at low magnification (b) at higher magnification (c) +100 mV at low magnification (d) at higher magnification (e) +600 mV at low magnification (f) at higher magnification.

At the anodic potentials of +100 mV and +600 mV, the friction curves were smoother and had near similar coefficient values of 0.28 and 0.25 respectively. Figures 6 (c-d) show the wear track at +100 mV whereas figures 6 (e-f) show the wear scar at +600 mV. The SEM images, figure 6c and 6e, show the area of the specimens exposed for experimentation at lower magnification. It appeared heavily corroded in both conditions. The corrosion currents (table 1) were extremely high (on average 3 orders of magnitude higher than for the coating). The wear track mainly consisted of some areas which exhibited grooving due to the ploughing action of the wear debris; however, it was dominated by the formation of corrosion products in the form of scales which appeared cracked. Thus, the SWC mechanisms for HSS specimens consisted of plastic deformation (ploughing) of the alloy, abrupt removal of the metal and its loosely attached corrosion products. The easy removal of these cracked and loosely adhered corrosion products were responsible for the drop in friction coefficient values and for a poor tribocorrosion resistance. The HSS specimens showed three orders of magnitude increase in wear coefficient at +100 mV ($K_c = 1.06 \times 10^{-12} \text{ m}^3\text{N}^{-1}\text{m}^{-1}$) and +600 mV ($K_c = 1.33 \times 10^{-12} \text{ m}^3\text{N}^{-1}\text{m}^{-1}$) as compared to the dry sliding wear coefficient of $K_c = 5.2 \times 10^{-15} \text{ m}^3\text{N}^{-1}\text{m}^{-1}$.

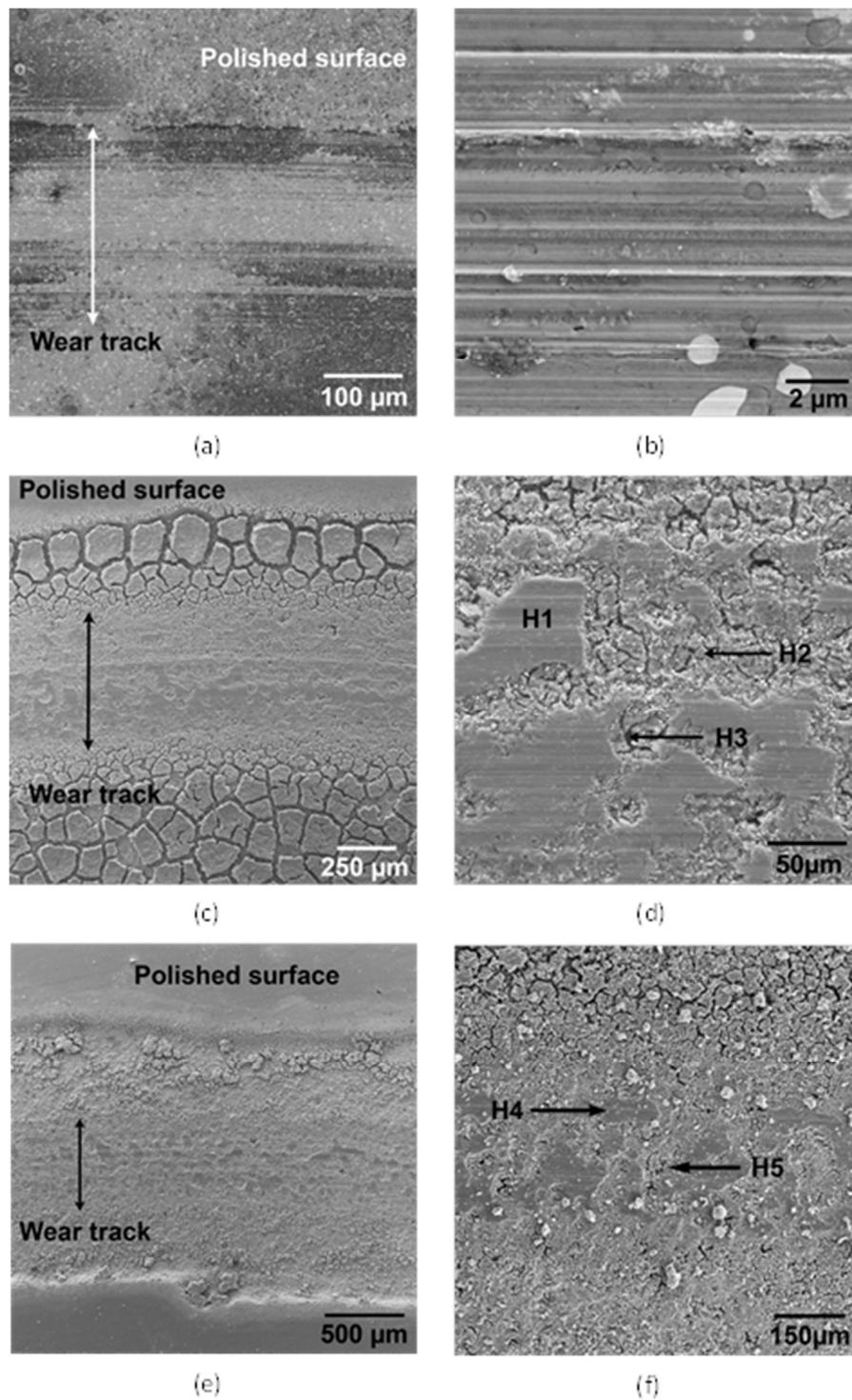


Figure 6: SEM images of the wear tracks on the HSS specimen: (a) -1200 mV at low magnification (b) at higher magnification (c) +100 mV at low magnification (d) at higher magnification (e) +600 mV at low magnification (f) at higher magnification.

The results of potentiodynamic as well as potentiostatic tribo-corrosion experiments on HSS indicate a strong effect of corrosion on wear and vice versa. Poor corrosion resistance of the alloy facilitates formation of corrosion products which are easily dislodged due to the mechanical action (siding ball); which in turn exposes fresh surface leading to further corrosion. This cyclic phenomenon of oxidation-removal-reoxidation is evident almost for all anodic potentials employed in this work. Wear rate as well as corrosion current measurements indicate a strong synergy between them. In comparison, CrN/NbN coating had (by 3 orders of magnitude) lower corrosion currents compared to HSS, showed a limited synergistic effect in the potential range of around +200 mV to +600 mV where a steady drop in the friction coefficient was observed. It is worth mentioning that the alumina counterpart showed minuscule wear and was beyond measurement in all the experiments conducted in this study.

Raman spectroscopy was used to identify any corrosion products formed on the surface. Raman spectra were obtained from different areas of the wear track (which were peculiar and anticipated to be associated with corrosion products). Figures 7a and 7b show the Raman spectra obtained from the wear track generated at +100 mV and +600 mV respectively. The surface features marked as C1 in the figure 5d and C3 in figure 5f were associated with the formation of a cavity in the coating due to the removal of deposition chamber related coating defects (dust from the chamber walls and fixtures). Depending on the depth to which they are embedded, they can facilitate the corrosive solution a direct path to the substrate [28] and lead to its corrosion. The general shape of Raman spectra recorded from these cavities resembled that of the coating suggesting the presence of coating underneath [29]. However, peaks associated with iron oxides were also visible and could be attributed to the corrosion of the substrate. Apart from these cavities, the wear track mostly resembled the coating (identified as spot C2 in figure 5d and most of the area in figure 5f) and showed strong peaks associated with

oxides of Cr and Nb which could be associated with the passive layers formed on the coating surface (corrosion products sustained after evading mechanical removal). Table 2 gives the resolved peak values of the Raman spectra for the coating and the HSS specimens and the assigned phases [29-36].

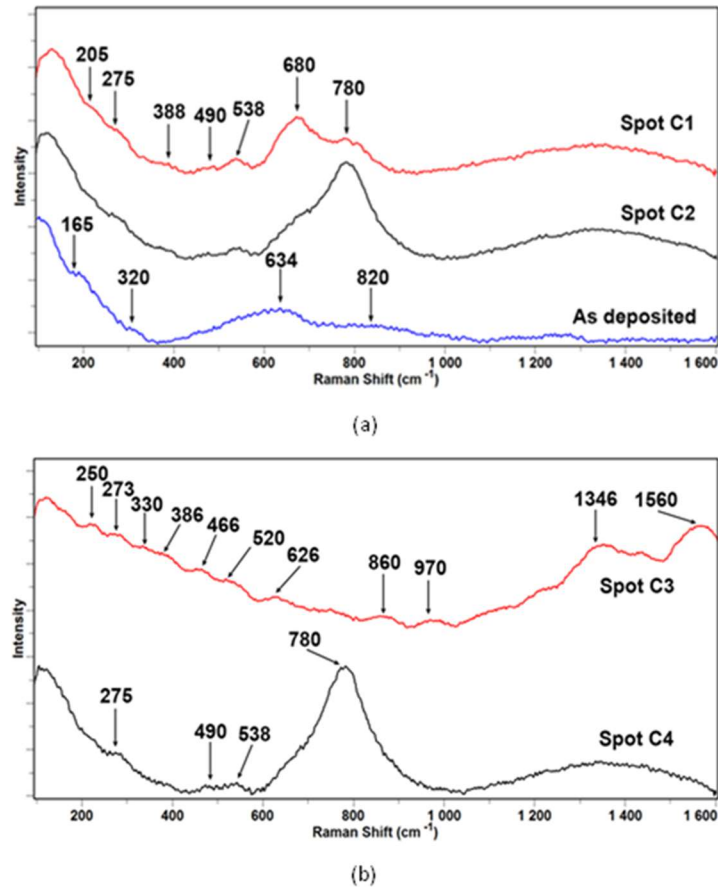
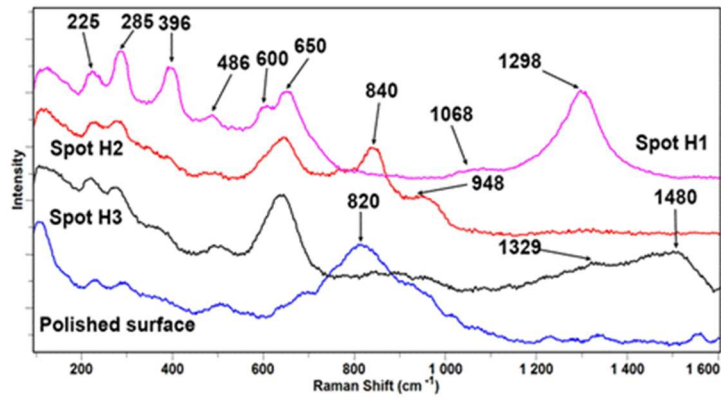


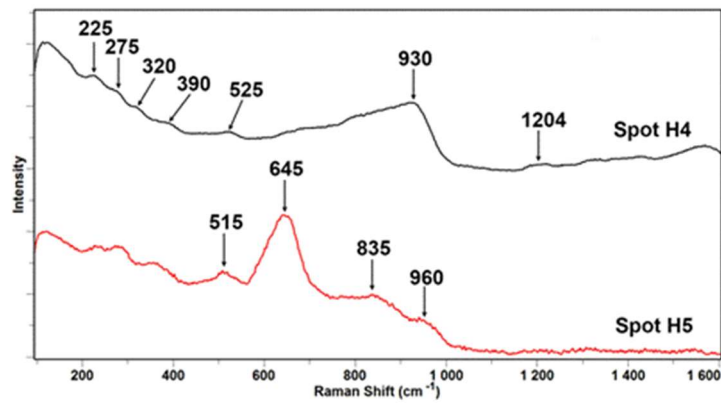
Figure 7: Raman spectra of the wear tracks features generated on the CrN/NbN coating: (a) +100 mV (b) +600 mV.

Similarly, Raman spectra of the HSS wear track were also analysed to identify the corrosion products. Figure 8a and 8b shows the spectra of the wear track for the HSS specimen generated at +100 mV and +600 mV respectively. Different features of these wear tracks have been identified as spots H1 to H4 (figures 6d and 6f). As anticipated, the Raman peaks were mainly associated with the different phases of iron oxides. Due to the complexity of the SWC process

and presence of alloying elements in the HSS as well as complex nature of coating architecture, overlapping peaks associated with different oxide phases of different elements could also be present and may have been left unidentified.



(a)



(b)

Figure 8: Raman spectra of the wear tracks features generated on the HSS specimen: (a)

+100 mV (b) +600 mV.

Specimen	Raman Frequencies (cm ⁻¹)	Peak Assignments
CrN/NbN	165, 320, 634, 820	CrN/NbN coating
	205, 275, 388, 490,	α -Fe ₂ O ₃ , Fe ₂ O ₃
	538, 680,	Cr ₂ O ₃ ,
	680,780,	Nb ₂ O ₅ / CrNbO ₄
	250, 330, 466, 520, 1346, 1560	Iron hydroxides (FeO(OH).H ₂ O)
	626, 860	CrN / Cr ₂ O ₃
	970	Nb ₂ O ₅
HSS	225, 285, 1329, 1480	α -Fe ₂ O ₃ , Fe ₂ O ₃
	396, 486, 515, 525, 930, 948, 960, 1068, 1298,	α -FeOOH.H ₂ O
	600, 650,	Cr ₂ O ₃ ,
	820, 835, 840,	CrO,

Table 2: Raman peaks and the main oxide phases identified on the surface of the wear track [29-36].

4.0 Conclusions:

A HIPIMS deposited nanoscale multilayer CrN/NbN coating and M2 HSS were investigated for their combined tribocorrosion resistance under sliding wear-corrosion conditions at 3 different electrochemical potentials with the help of a pin-on disk apparatus. In this study, the alumina counterpart exhibited negligible wear. Under the test parameters employed, following inferences about the CrN/NbN coating and uncoated HSS can be drawn:

- 1) The CrN/NbN coating had a low wear coefficient ($K_c = 1.39 \times 10^{-15} \text{ m}^3\text{N}^{-1}\text{m}^{-1}$) as compared to the HSS ($K_C = 5.29 \times 10^{-15} \text{ m}^3\text{N}^{-1}\text{m}^{-1}$) in dry sliding wear conditions.
- 2) At cathodic conditions and under aqueous lubrication conditions, the nanoscale CrN/NbN multilayer coating retains its unique layer by layer wear mechanism and thus a low coefficient of wear, $K_c = 2 \times 10^{-15} \text{ m}^3\text{N}^{-1}\text{m}^{-1}$ (high wear resistance).
- 3) For the anodic potentials investigated, corrosion products formed during the sliding wear process had a limited influence on the friction coefficient values of the coating.

The results indicate superior performance in terms of better corrosion resistance and structural integrity of the coating and oxides formed at those potentials indicating a lower synergy between corrosion and wear. In comparison, friction coefficient values of the HSS were significantly affected by the loose corrosion products.

- 4) Under extreme tribo-corrosive conditions (consisting of anodic potentials of +100 mV and +600 mV) the CrN/NbN coated substrates had lower corrosion currents and lower material removal rates suggesting a superior tribocorrosion resistance. In comparison, uncoated HSS specimens exhibited three orders of magnitude higher corrosion currents as well as material loss. In this study, the chamber related dust was found to have no significant effect on the tribo-corrosion resistance of the coating.
- 5) The superior performance of the CrN/NbN coating can be attributed to high adhesion, dense columnar structure, inherent hardness and toughness of the superior nanoscale multilayer architecture achieved due to the HIPIMS deposition technique.

Conflict of Interest: The authors declare that they have no conflict of interest.

References

- [1] S. Zhou, M.M. Stack, R.C. Newman (1996) Characterization of Synergistic Effects Between Erosion and Corrosion in an Aqueous Environment Using Electrochemical Techniques, *CORROSION* 52 (12): 934-946.
- [2] M.M. Stack (2002) Mapping tribo-corrosion processes in dry and aqueous conditions: some new directions for the new Millennium, *Tribology International* 35: 681-689.
- [3] M.M. Stack and K. Chi (2003) Mapping sliding wear of steels in aqueous conditions, *Wear* 255: 456-465.
- [4] R.J.K. Wood (2017) Marine wear and tribocorrosion, *Wear* 376-377: 893-910.
- [5] Y. Yan, A. Neville, D. Dowson, S. Williams (2006) Tribocorrosion in implants—assessing high carbon and low carbon Co–Cr–Mo alloys by in situ electrochemical measurements, *Tribology International* 39:1509-1517.
- [6] M.M. Stack, M.T. Mathew, C. Hodge (2011) Micro-abrasion–corrosion interactions of Ni–Cr/WC based coatings: Approaches to construction of tribo-corrosion maps for the abrasion–corrosion synergism, *Electrochimica Acta* 56: 8249-8259.
- [7] J. Jiang, M.M. Stack, A. Neville (2002) Modelling the tribo-corrosion interaction in aqueous sliding conditions, *Tribology International* 35: 669-679.
- [8] S. Cao and S. Mischler (2018) Modeling tribocorrosion of passive metals – A review, *Current Opinion in Solid State and Materials Science* 22: 127-141.
- [9] P.E. Hovsepian, D.B. Lewis, W.-. Müunz, A. Rouzaud, P. Juliet (1999) Chromium nitride/niobium nitride superlattice coatings deposited by combined cathodic-arc/unbalanced magnetron technique, *Surface and Coatings Technology* 116-119: 727-734.

- [10] P.E. Hovsepian, D.B. Lewis, W.D. Münz, S.B. Lyon, M. Tomlinson (1999) Combined cathodic arc/unbalanced magnetron grown CrN/NbN superlattice coatings for corrosion resistant applications, *Surface and Coatings Technology* 120-121: 535-541.
- [11] P.E. Hovsepian, D.B. Lewis, Q. Luo, W.-. Münz, M. Meyer (1999) *Surface Engineering, Euromat proceedings* 11: 41-46.
- [12] V. Kouznetsov, K. Macák, J.M. Schneider, U. Helmersson, I. Petrov (1999) A novel pulsed magnetron sputter technique utilizing very high target power densities, *Surface and Coatings Technology* 122: 290-293.
- [13] A.P. Ehasarian, R. New, W.-. Münz, L. Hultman, U. Helmersson, V. Kouznetsov (2002) Influence of high power densities on the composition of pulsed magnetron plasmas, *Vacuum* 65: 147-154.
- [14] A.P. Ehasarian, W.-. Münz, L. Hultman, U. Helmersson, I. Petrov (2003) High power pulsed magnetron sputtered CrN_x films, *Surface and Coatings Technology* 163-164: 267-272.
- [15] A. P. Ehasarian, J. G. Wen, I. Petrov (2007) Interface microstructure engineering by high power impulse magnetron sputtering for the enhancement of adhesion, *J. Apply. Phys.* 101: 054301-054310.
- [16] Y.P. Purandare, A.P. Ehasarian, P.E. Hovsepian (2008) Deposition of nanoscale multilayer CrN/NbN physical vapor deposition coatings by high power impulse magnetron sputtering, *Journal of Vacuum Science & Technology A: Vacuum, Surfaces, and Films* 26 (2): 288-296.
- [17] P.E. Hovsepian, A.P. Ehasarian, Y.P. Purandare, R. Braun, I.M. Ross (2009) Effect of High Ion Irradiation on the Structure, Properties and High Temperature Tribology of Nanoscale CrAlYN/CrN Multilayer Coating Deposited by HIPIMS-HIPIMS Technique, *Plasma Processes and Polymers* 6 (S1): S118-S123.

- [18] Y.P. Purandare, A.P. Ehiasarian, M.M. Stack, P.E. Hovsepian (2010) CrN/NbN coatings deposited by HIPIMS: A preliminary study of erosion–corrosion performance, *Surface and Coatings Technology* 204: 1158-1162.
- [19] P.E. Hovsepian, A.P. Ehiasarian, Y.P. Purandare, B. Biswas, F.J. Pérez, M.I. Lasanta, M.T. de Miguel, A. Illana, M. Juez-Lorenzo, R. Muelas, A. Agüero (2016) Performance of HIPIMS deposited CrN/NbN nanostructured coatings exposed to 650° C in pure steam environment, *Materials Chemistry and Physics* 179: 110-119.
- [20] P.E. Hovsepian, A.P. Ehiasarian, Y.P. Purandare, P. Mayr, K.G. Abstoss, M. Mosquera Feijoo, W. Schulz, A. Kranzmann, M.I. Lasanta, J.P. Trujillo (2018) Novel HIPIMS deposited nanostructured CrN/NbN coatings for environmental protection of steam turbine components, *Journal of Alloys and Compounds* 746: 583-593.
- [21] P.E. Hovsepian, A.P. Ehiasarian, Y. Purandare, A.A. Sugumaran, T. Marriott, I. Khan (2016) Development of superlattice CrN/NbN coatings for joint replacements deposited by high power impulse magnetron sputtering, *Journal of Materials Science: Materials in Medicine*, 27: 147 (1-10).
- [22] H. Holleck and V. Schier (1995) Multilayer PVD coatings for wear protection, *Surface and Coatings Technology* 76-77: 328-336.
- [23] Marcel Pourbaix (1974) *Atlas of Electrochemical Equilibria in Aqueous Solutions*, NACE International, Cebelcor.
- [24] D. Landolt, S. Mischler, M. Stemp (2001) Electrochemical methods in tribocorrosion: a critical appraisal, *Electrochimica Acta* 46: 3913-3929.
- [25] K. Kato (2011) *Friction and wear of passive metals and coatings*. Woodhead Publishing, Cambridge, UK, pp 65-99.

- [26] B. Biswas, Y. Purandare, A.A. Sugumaran, D.A.L. Loch, S. Creasey, I. Khan, A.P. Ehiasarian, P.E. Hovsepian (2017) Defect growth in multilayer chromium nitride/niobium nitride coatings produced by combined high power impulse magnetron sputtering and unbalance magnetron sputtering technique, *Thin Solid Films* 636: 558-566.
- [27] V. Dalbert, N. Mary, B. Normand, C. Verdu, T. Douillard, S. Saedlou (2019) The effects of microstructures and repassivation kinetics on the tribocorrosion resistance of ferrite and ferrite-martensite stainless steels, *Wear* 420-421: 245-256.
- [28] H.W. Wang, M.M. Stack, S.B. Lyon, P. Hovsepian, W.-. Münz (2000) The corrosion behaviour of macroparticle defects in arc bond-sputtered CrN/NbN superlattice coatings, *Surface and Coatings Technology* 126: 279-287.
- [29] Constable, C.P. (2000), Raman microscopic studies of PVD deposited hard ceramic coatings. PhD thesis, Sheffield Hallam University.
- [30] H.C. Barshilia and K.S. Rajam (2004) Raman spectroscopy studies on the thermal stability of TiN, CrN, TiAlN coatings and nanolayered TiN/CrN, TiAlN/CrN multilayer coatings, *J. Mater. Res.* 19 (11): 3196-3205.
- [31] M. Criado, S. Martínez-Ramirez, J.M. Bastidas (2015) A Raman spectroscopy study of steel corrosion products in activated fly ash mortar containing chlorides, *Construction and Building Materials* 96: 383-390.
- [32] X. Zhang, K. Xiao, C. Dong, J. Wu, X. Li, Y. Huang (2011) In situ Raman spectroscopy study of corrosion products on the surface of carbon steel in solution containing Cl^- and SO_4^{2-} , *Engineering Failure Analysis* 18: 1981-1989.
- [33] S. Ramya, T. Anita, H. Shaikh, R.K. Dayal (2010) Laser Raman microscopic studies of passive films formed on type 316LN stainless steels during pitting in chloride solution, *Corrosion Science* 52: 2114-2121.

- [34] H.C. Barshilia, K.S. Rajam, A. Jain, K. Gopinadhan, S. Chaudhary (2006) A comparative study on the structure and properties of nanolayered TiN/NbN and TiAlN/TiN multilayer coatings prepared by reactive direct current magnetron sputtering, *Thin Solid Films* 503: 158-166.
- [35] C.P. Constable, J. Yarwood, P. Hovsepian, L.A. Donohue, D.B. Lewis, W.-. Münz (2000) Structural determination of wear debris generated from sliding wear tests on ceramic coatings using raman microscopy, *J. Vac. Sci. Technol.* 18 (4): 1681-1689.
- [36] G.A. Fontalvo, V. Terziyska, C. Mitterer (2007) High-temperature tribological behaviour of sputtered NbN_x thin films, *Surface and Coatings Technology* 202: 1017-1022.

Figure captions

Figure 1: Schematic representation of the Sliding wear-corrosion set up.

Figure 2: SEM images of the CrN/NbN coating captured in secondary electron imaging mode: (a) plan view showing as deposited surface (b) Cross-sectional view (c) Bright field TEM image showing nanoscale alternating CrN (light contrast area) NbN (dark contrast) layers.

Figure 3: Polarisation curves, friction coefficient measurement as a function of sliding distance under a normal load of 5N (a) CrN/NbN coating (b) M2 HSS specimen.

Figure 4: Friction coefficient as a function of electrochemical potentials under sliding wear conditions under a normal load of 5N (a) CrN/NbN coating (b) M2 HSS specimen.

Figure 5: SEM images of the wear tracks on the CrN/NbN coating: (a) -1200 mV at low magnification (b) at higher magnification (c) +100 mV at low magnification (d) at higher magnification (e) +600 mV at low magnification (f) at higher magnification.

Figure 6: SEM images of the wear tracks on the HSS specimen: (a) -1200 mV at low magnification (b) at higher magnification (c) +100 mV at low magnification (d) at higher magnification (e) +600 mV at low magnification (f) at higher magnification.

Figure 7: Raman spectra of the wear tracks features generated on the CrN/NbN coating: (a) +100 mV (b) +600 mV.

Figure 8: Raman spectra of the wear tracks features generated on the HSS specimen: (a) +100 mV (b) +600 mV.

Table captions

Table 1: Mean friction coefficient, corrosion currents and wear coefficients measured as a function of electrochemical potentials and sliding distance under a normal load of 5N.

Table 2: Raman peaks and the main oxide phases identified on the surface of the wear track [29-36].